Peptide Free-Energy Profile Is Strongly Dependent on the Force Field: Comparison of C96 and AMBER95

SATOSHI ONO, NOBUYUKI NAKAJIMA,* JUNICHI HIGO, HARUKI NAKAMURA†

Biomolecular Engineering Research Institute, 6-2-3 Furuedai, Suita, Osaka 565-0874, Japan

Received 30 April 1999; accepted 3 February 2000

ABSTRACT: The C96 and AMBER95 force fields were compared with small model peptides Ac-$(Ala)_n$-NMe (Ac = CH_3CO, NMe = $NHCH_3$, $n = 2$ and 3) *in vacuo* and in TIP3P water by computing the free-energy profiles using multicanonical molecular dynamics method. The C96 force field is a modified version of the AMBER95 force field, which was adjusted to reproduce the energy difference between extended β- and constrained α-helical energies for the alanine tetrapeptide, obtained by the high level *ab initio* MO method. The slight modification resulted in a large difference in the free energy profiles. The C96 force field prefers relatively extended conformers, whereas the AMBER95 force field favors turn conformations. © 2000 John Wiley & Sons, Inc. J Comput Chem 21: 748–762, 2000

Keywords: force field; multicanonical molecular dynamics; alanine peptide; AMBER95 force field; C96 force field

Introduction

The AMBER95 force field,[1] which is sometimes referred to as AMBER 4.1 or parm94.dat, has been applied to a wide variety of peptides, proteins, and nucleic acids. Beachy et al.[2] studied 10 local minima of alanine tetrapeptides with a high level *ab initio* molecular orbital (MO) method, and compared their results to those of existing force fields, including the AMBER95 force field. Although these conformers rarely occur in protein crystal structures, it was found that the AMBER95 force field did not reproduce the *ab initio* results well. Kollman et al. modified the AMBER95 force field to reproduce the *ab initio* MO $\alpha_R - \beta$ energy difference exactly, and they named this modification the C96 force field.[3] Equation (1) represents the functional form of a force field, as usually intended.[1] The differences between AMBER95 and C96 lie only in the backbone dihedral parameters. In the AMBER95 force field, the dihedral parameters in eq. (1) are $V_2/2 = 0.2$ kcal mol^{-1} and $\delta_2 = 180°$ for around

Correspondence to: H. Nakamura; e-mail: harukin@protein.osaka-u.ac.jp

*Present address: Mitsubishi Chemical Corporation

†Present address: Institute for Protein Research, Osaka University, 3-2 Yamadaoka, Suita, Osaka 565-0871, Japan

C—N—CT—C(ϕ), $V_1/2 = 0.75$, $\delta_1 = 180°$, $V_2/2 = 1.35$, $\delta_2 = 180°$, and $V_4/2 = 0.40$, $\delta_4 = 180°$ for around N—C—CT—N(ψ). In the C96 force field, for around both C—N—CT—C and N—C—CT—N, the parameters are changed to $V_1/2 = 0.85$ kcal mol^{-1}, $\delta_1 = 0°$ and $V_2/2 = 0.30$, $\delta_2 = 180°$. The remaining parameters are identical to those of the AMBER95 force field.

$$E_{\text{total}} = \sum_{\text{bonds}} K_r(r - r_{\text{eq}})^2 + \sum_{\text{angles}} K_\theta(\theta - \theta_{\text{eq}})^2 + \sum_{\text{dihedrals}} \frac{V_n}{2}\left[1 + \cos(n\phi - \delta_n)\right] + \sum_{i<j}\left[\frac{A_{ij}}{R_{ij}^{12}} - \frac{B_{ij}}{R_{ij}^{6}} + \frac{q_i q_j}{\epsilon R_{ij}}\right] \quad (1)$$

This change led to a significant improvement in the agreement between the molecular mechanical and quantum mechanical relative energies for the test set of 10 conformations of the alanine tetrapeptide.[3] Kollman et al.[3] confirmed the availability of the C96 force field with isolated ubiquitin and blocked poly-L-leucine in solution. In the case of ubiquitin, the overall rmsd differences between the C96 and AMBER95 force field and the crystal structure were not significant, whereas the free energy profiles of blocked poly-L-leucine along the backbone dihedral angle ψ and the O_i—H_{i+3} distance were different between the C96 and AMBER95 force fields. The C96 force field slightly stabilizes the β conformations and the transition state between the α_R and β conformations.

Figure 1 shows the potential map of an alanine dipeptide Ac-Ala-NMe (Ac = CH_3CO and NMe = $NHCH_3$) for the C96 and AMBER95[1] force fields and the differences between them in the gas phase. These potentials are different for key areas of peptides and proteins. The $C7_{eq}$ conformation, which has a seven-atom ring closed by a hydrogen bond, is the most stable conformer for both force fields, and it is placed at $(\phi, \psi) = (-74, 75)$ for C96, and at $(-73, 66)$ for AMBER95. A nearly extended structure, which has a strained internal hydrogen bond in a five-atom ring, called the C5 conformation, is placed at $(-148, 160)$ and $(-147, 171)$ for C96 and AMBER95, respectively. The energy differences between the $C7_{eq}$ and C5 conformations are 0.2 kcal mol^{-1} and 1.5 kcal mol^{-1} for the C96 and AMBER95 force fields.[3] The difference obtained by one of the highest levels of *ab initio* quantum mechanical calculations by "MP4-BSSE"/cc-pVTZ(-f)//MP2/6-31G* was reported to be 0.89 kcal mol^{-1}.[2] In the alanine dipeptide, the α-helical region α_R has no stable point in the both force fields.

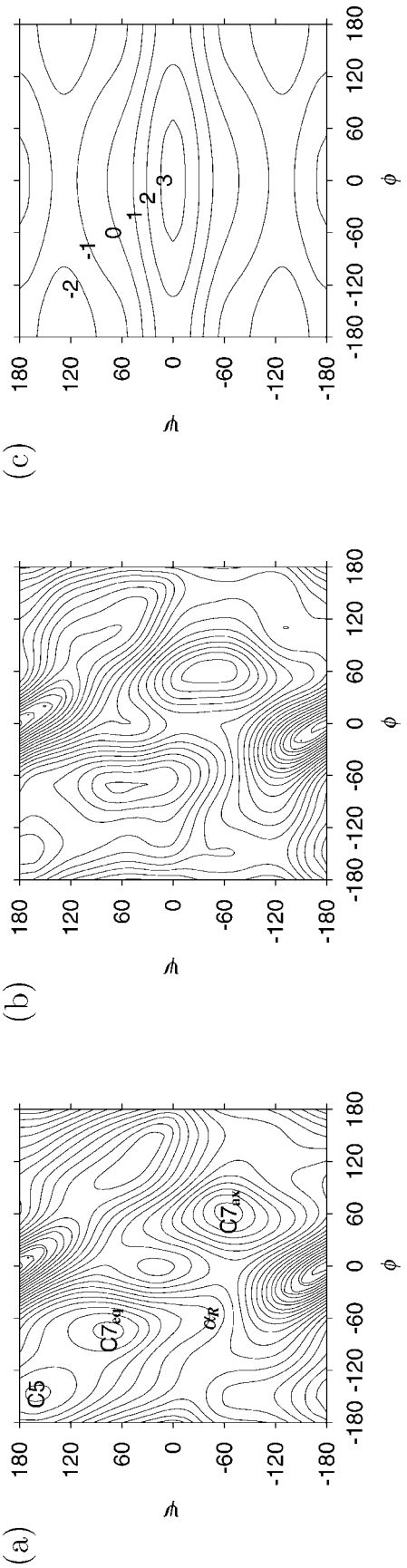

FIGURE 1. Potential map of the alanine dipeptide Ac-Ala-NMe (a) for C96, (b) for AMBER95, and (c) the difference map between C96 and AMBER95. These maps were calculated by molecular mechanics in the gas phase, by constraining the (ϕ, ψ) with 10° steps, and the other degrees of freedom were relaxed and were optimized. The contours are plotted with 1 kcal mol^{-1} intervals. α_R is labeled at $(\phi, \psi) = (-60.7, -40.7)$.

The energy differences between $C7_{eq}$ and the constrained α_R with $(\phi, \psi) = (-60.7, -40.7)$ are 5.4 and 3.8 kcal mol^{-1} for C96 and AMBER95, respectively. The slope between $C7_{eq}$ and α_R is steeper for AMBER95 than for C96, and the hollow of $C7_{eq}$ seems to extend to the α_R region for AMBER95. Another stable region in the potential surface of the alanine dipeptide is the $C7_{ax}$ region, which is placed at $(\phi, \psi) = (62, -66)$ for C96 and at $(61, -53)$ for AMBER95. The energy differences between $C7_{eq}$ and $C7_{ax}$ are 1.9 kcal mol^{-1} and 1.5 kcal mol^{-1} for C96 and AMBER95, respectively. They are much smaller than the *ab initio* result, 2.55 kcal mol^{-1}.[2]

However, there have been no systematic investigation to reveal the characteristics of those two force field from the free energy analysis. In this study, we have chosen small blocked alanine peptides Ac-$(Ala)_n$-NMe ($n = 2$ and 3), as a model system for testing the differences between the C96 and AMBER95 force fields with a multicanonical method, which can effectively sample the conformational energy space to reveal the free energy profile. These simple peptides have been studied by many researchers using a variety of computational methods. For example, the blocked alanine dipeptide (Ac-Ala-NMe) has been studied extensively, by *ab initio* MO, Monte Carlo (MC) and molecular dynamics (MD) (see refs. 4 and 5). For longer peptide, simulations have been done for Ac-$(Ala)_2$-NMe[6,7] and Ac-$(Ala)_3$-NMe[8–10] by umbrella sampling, to obtain the free energy surfaces.

The multicanonical algorithm was first proposed by Berg and Neuhaus[11] to improve the sampling efficiency in an effective MC simulation, and it has been applied to a variety of systems, such as the conformational sampling of small peptides.[12–16] To overcome the disadvantages in MC simulations of proteins,[15] Nakajima et al.[17] developed the multicanonical algorithm in an MD simulation in Cartesian space to obtain the multicanonical ensemble, and it was applied to the flexible docking of a ligand peptide[18] and CDR-H3.[19] These results showed that the multicanonical MD sampled a much larger conformational space than the conventional MD. Recently, in an explicit water molecule system, the selectively enhanced multicanonical method was proposed, which selectively enhances the sampling efficiency in the energy space for the solute–solute and solute–water interactions by using the multicanonical algorithm, while it restrains the sampling of the water–water energy space. When applied to Ac-$(Gly)_2$-NMe and Ac-$(Ala)_2$-NMe in water, much less computation time was required for the selectively enhanced multicanonical method than for the conventional method, and the distributions at room temperature were in good agreement.[20]

Methods

MULTICANONICAL MD

Here, the multicanonical MD method[17] is described briefly. The probability distribution, P_c, of the potential energy, E, for the canonical ensemble at a temperature, T, is given by

$$P_c(E,T) = \frac{1}{Z_c} n(E) \exp(-E/kT) \tag{2}$$

where k is the Boltzmann constant, $n(E)$ is the density of states, and $Z_c = \sum_E n(E) \exp(-E/kT)$. To overcome the high conformational energy barrier at room temperature, the multicanonical ensemble is introduced, which produces a flat energy distribution, P_{mc}, as

$$P_{mc}(E) = \frac{1}{Z_{mc}} n(E) \exp\big[-W(E)\big] = \text{constant} \tag{3}$$

Here, $W(E)$ is the weight function of E, and $Z_{mc} = \sum_E n(E) \exp[-W(E)]$. This flat energy distribution enables us to overcome the potential energy barriers by sufficiently sampling the high-energy regions and also to obtain the statistically significant distributions at a low temperature by fully sampling the low-energy regions. After the simulation, the reweighting formula derived from eqs. (2) and (3) converts P_{mc} into a canonical distribution, P_c, at an arbitrary temperature, T, as

$$\begin{aligned} P_c(E,T) &= \frac{1}{Z_c} n(E) \exp(-E/kT) \\ &= \frac{Z_{mc}}{Z_c} P_{mc}(E) \exp\big[W(E) - E/kT\big] \end{aligned} \tag{4}$$

The function $W(E)$ is not given *a priori*, but is determined from a preliminary canonical simulation at sufficiently high temperature, T_0, as,

$$W(E) = \ln n(E) = (E/kT_0) + \ln P_c(E, T_0) \tag{5}$$

where the energy-independent terms are neglected. When $P_c(E, T_0)$ does not cover a sufficiently large E range, the weight function, $W(E)$, can be refined iteratively with several multicanonical MD runs by using following relation,

$$W^{i+1}(E) = W^i(E) + \ln P^i_{mc}(E) \tag{6}$$

where the ith multicanonical distribution, $P^i_{mc}(E)$, is derived from the weight function $W^i(E)$.

In the selectively enhanced multicanonical method,[20] the energy is separated into two components, $E = E_A + E_B$, where E_A is the solute–solute

and solute–water interaction energy, and E_B is the water–water interaction energy. For both the E_A and E_B spaces, flat energy distributions are obtained in the same manner, as described above. For the E_B space, the energy barriers should be lower than those in the E_A space, and the sampling of the E_B space can be restricted by the room temperature, T_1.

COMPUTATIONS

The all-atom C96[3] and AMBER95[1] force fields were used. The program PRESTO[21] was used for the potential calculations and the MD simulations.

The blocked alanine peptides, Ac-$(Ala)_n$-NMe ($n = 2$ and 3), *in vacuo* and in bulk water, were analyzed by multicanonical MD. The extended conformation was used as an initial structure. The nonbonded interactions were not truncated *in vacuo*, and the nonbonded interactions longer than 12 Å were truncated in the water simulations. In bulk water, the solute was placed at the center of a sphere with the TIP3P water model.[22] The radii of the spheres for $n = 2$ and $n = 3$ were 12 and 14 Å, respectively, which correspond to the addition of, at least, about three water layers to the both sides of the peptide. The numbers of water molecules were 219 and 367, respectively. The CAP constraint was used. All simulations were performed with a constant temperature MD by the constraint method,[23, 24] where the total kinetic energy was always constant, and the equation of motions was integrated by the leap-frog method. The time step was 0.5 fs for *in vacuo* simulations, and 1.0 fs for in water simulations. The SHAKE[25] method was used in the water calculation to constrain the bonds between heavy atoms and hydrogen atoms. First, a canonical simulation was performed at $T_0 = 700$ K. In the selectively enhanced multicanonical MD, the water–water interactions were performed at $T_1 = 310$ K, and the temperatures for E_A and E_B were controlled separately. The final MD calculations were carried out for 1×10^7 steps. With several iterations of multicanonical MDs, typically three to four times *in vacuo* and six to eight times in water, canonical distributions at 300 K were obtained by the reweighting formula, eq. (4). Tables I and II indicate the refined $W(E)$ functions, which were fitted and extrapolated by polynomial functions.[15] The potentials of mean force, A, along the O—H distances, r, were calculated by the equation $A(r) = -kT \ln P(r)$ at room temperature, $T = 300$ K. An additional MD run for Ac-$(Ala)_3$-NMe with an initial structure O_1—$H_5 = 6$ Å in water for the AMBER95 force field was carried out for 1×10^7 steps to examine the convergence of the simulations.

Results and Discussion

ENERGY TRAJECTORIES

Figures 2a and b show the energy trajectories of Ac-$(Ala)_3$-NMe *in vacuo* for the C96 and AMBER95 force fields, respectively. Both trajectories yield a flat probability distribution, shown in Figure 2c. Figure 2d shows the energy distributions of Ac-$(Ala)_3$-NMe in water for the E_A and E_B components. Both components yielded the flat probability distributions for the AMBER95 and C96 force fields. This indicates that the simulations were successfully performed to produce the multicanonical ensemble. However, low energy regions appeared and stayed for some time with C96 force field *in vacuo*, while the simulation for AMBER95 evenly sampled the energy space. For C96, another calculation with 6×10^7 steps was carried out. However, the energy trajectory and probability distribution for each group of 1×10^7 steps were almost identical. The thermodynamic property obtained from these energy trajectories will be discussed later.

ALANINE TRIPEPTIDE

In Figure 3a, the free energy profile of the alanine tripeptide, Ac-$(Ala)_2$-NMe, for the C96 force field and the AMBER95 force field in the gas phase is presented as a function of the O_1—H_4 distance. Figure 4 shows the (ϕ, ψ) probability distribution map of each alanine residue. Apparently, C96 preferred the extended conformation with local minima along O_1—H_4 at 8.8 and 6.6 Å, while AMBER95 has the lowest local minimum at 2 Å, which indicates the high probability of the existence of the O_1—H_4 hydrogen bond (Fig. 3a). The free energy of the extended conformation is 4.0 kcal mol^{-1} higher than that of the hydrogen-bonded conformation for AMBER95. The C96 profile also has a local minimum at 2 Å, but it is 2.0 kcal mol^{-1} higher than that of the extended conformation. Figure 5 shows the snap shots of the structures at these local minima.

The probability distribution for C96 (ϕ, ψ) is similar to the alanine dipeptide potential map, which has the main peaks located at $C7_{eq}$ and C5 (β region). In contrast, for AMBER95, the main peaks are located at $(\phi_2, \psi_2) = (-60, -5)$ and $(\phi_3, \psi_3) = (-70, -10)$, which correspond to Type I turn conformers, as illustrated in Figure 5a. Both force fields

TABLE I.

The Parameters for the Refined $W(E)$ Functions for the Simulations *in vacuo*.

	Ac-$(Ala)_2$-NMe		Ac-$(Ala)_3$-NMe	
Coefficients[a]	AMBER95	C96	AMBER95	C96
n	8	8	8	8
C_0	−0.14765E+02	−0.16032E+02	−0.26393E+02	−0.32425E+02
C_1	0.87363E+00	0.97265E+00	0.12140E+01	0.14638E+01
C_2	−0.26439E−01	−0.29742E−01	−0.31614E−01	−0.35917E−01
C_3	0.64106E−03	0.84402E−03	0.78271E−03	0.92106E−03
C_4	−0.21899E−04	−0.34696E−04	−0.17947E−04	−0.24456E−04
C_5	0.66096E−06	0.10573E−05	0.27484E−06	0.43947E−06
C_6	−0.12269E−07	−0.18194E−07	−0.24659E−08	−0.45962E−08
C_7	0.11902E−09	0.15941E−09	0.11585E−10	0.25275E−10
C_8	−0.46313E−12	−0.55549E−12	−0.21728E−13	−0.56497E−13
E^L [b]	−30.0	−45.0	−15.0	−20.0
E^H [b]	40.0	36.0	58.0	60.0

[a] Each logarithm of the probability function $P_c(E)$ in eq. (5) was fitted and extrapolated by polynomial function, $\sum_{i=0}^{n} C_i E^i$ to derive the refined $W(E)$ function.

[b] The parameters E^L and E^H are the connecting points between the polynomial function and the linear functions, $C_0 + C_1(E - E^L)$ and $C_0 + C_1(E - E^H)$, to avoid the oversampling of very low and high energy regions, respectively. The unit of the energies is kcal mol^{-1}.

TABLE II.

The Parameters for the Refined $W(E)$ Functions for the Simulations in Water.

	Ac-$(Ala)_2$-NMe		Ac-$(Ala)_3$-NMe	
Coefficients[a]	AMBER95	C96	AMBER95	C96
n	6	6	6	6
C_{0A}	−0.49988E+01	−0.50275E+01	−0.40342E+01	−0.40410E+01
C_{1A}	−0.16782E+00	−0.17357E+00	−0.94510E−01	−0.98068E−01
C_{2A}	−0.32910E−02	−0.37388E−02	−0.30873E−02	−0.31942E−02
C_{3A}	0.32196E−04	0.11672E−04	0.16079E−04	0.16869E−04
C_{4A}	0.17952E−07	−0.43554E−06	−0.53777E−07	−0.75976E−07
C_{5A}	0.38677E−10	−0.35666E−08	0.13064E−09	−0.68316E−09
C_{6A}	0.25561E−11	−0.70003E−11	0.38074E−11	−0.58396E−12
E_A^L [b]	−110.0	−105.0	−120.0	−120.0
E_A^H [b]	−19.0	−19.0	−13.0	−13.0
n	4	4	4	4
C_{0B}	0.13226E+04	−0.14524E+05	0.10488E+06	−0.27853E+05
C_{1B}	0.39098E+01	−0.30362E+02	0.13054E+03	−0.34718E+02
C_{2B}	0.30721E−02	−0.24678E−01	0.60384E−01	−0.16774E−01
C_{3B}	0.74445E−06	−0.92284E−05	0.12295E−04	−0.37148E−05
C_{4B}	0.89961E−11	−0.13333E−08	0.92908E−09	−0.31666E−09
E_B^L [b]	−1980.0	−1970.0	−3320.0	−3310.0
E_B^H [b]	−1820.0	−1830.0	−3130.0	−3118.0

[a] The logarithms of the probability functions $P_c(E_A)$ and $P_c(E_B)$, were fitted and extrapolated by polynomial functions, $\sum_{i=0}^{n} C_{iA} E_A^i$ and $\sum_{i=0}^{n} C_{iB} E_B^i$, respectively.

[b] The parameters E_X^L and E_X^H (X = A or B) are the connecting points between the polynomial function and the linear functions, $C_{0X} + C_{1X}(E_X - E_X^L)$ and $C_{0X} + C_{1X}(E_X - E_X^H)$, to avoid the oversampling of very low and high energy regions, respectively.

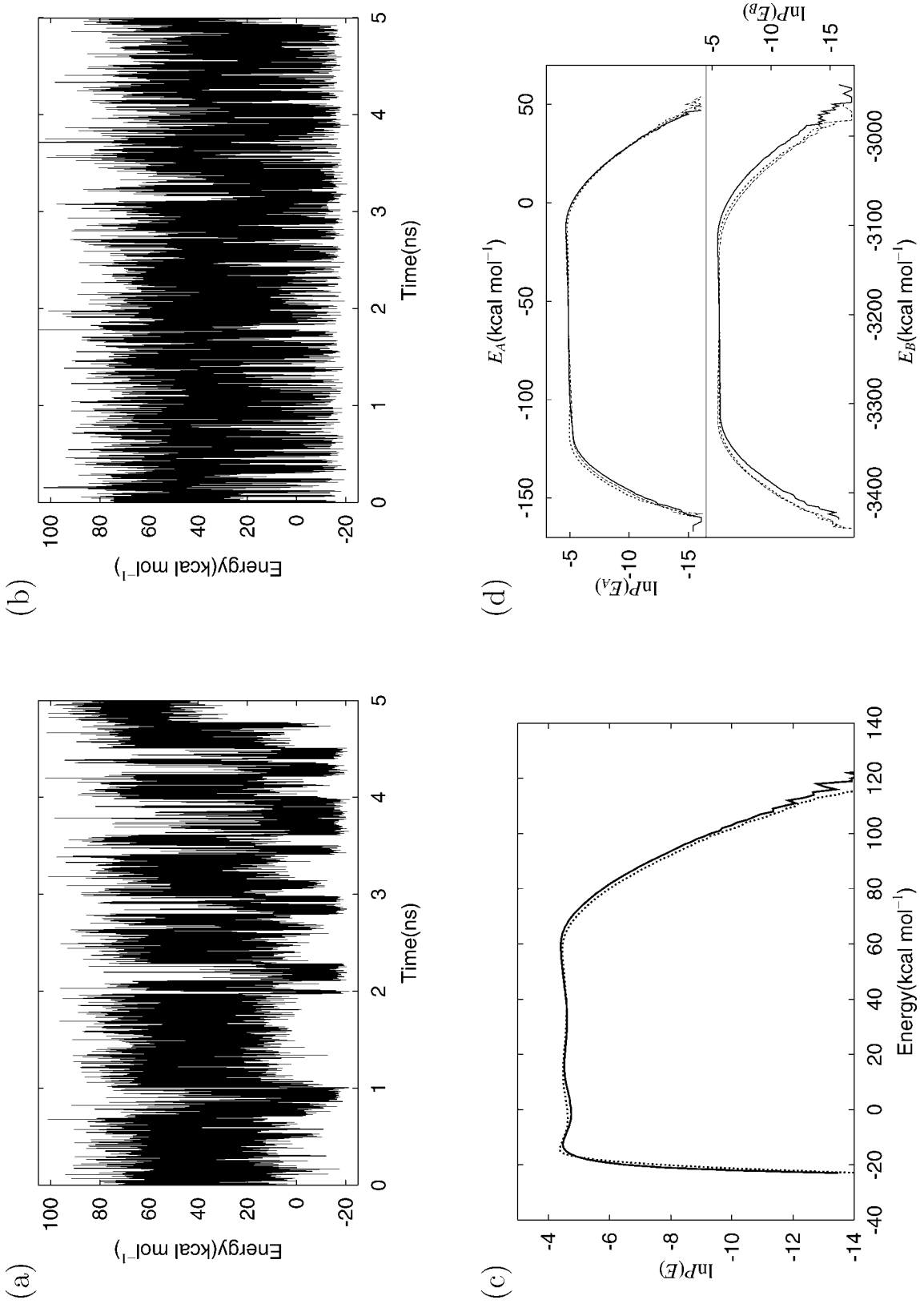

FIGURE 2. Energy trajectories of Ac-$(Ala)_3$-NMe *in vacuo* for (a) C96, (b) AMBER95, and (c) flat energy distributions for C96 (solid line) and AMBER95 (dotted line) obtained by the energy trajectories. (d) Flat energy distributions for E_A and E_B components in water for C96 (solid lines), AMBER95 (dotted lines), and an additional 10 ns simulation for AMBER95 (dashed lines).

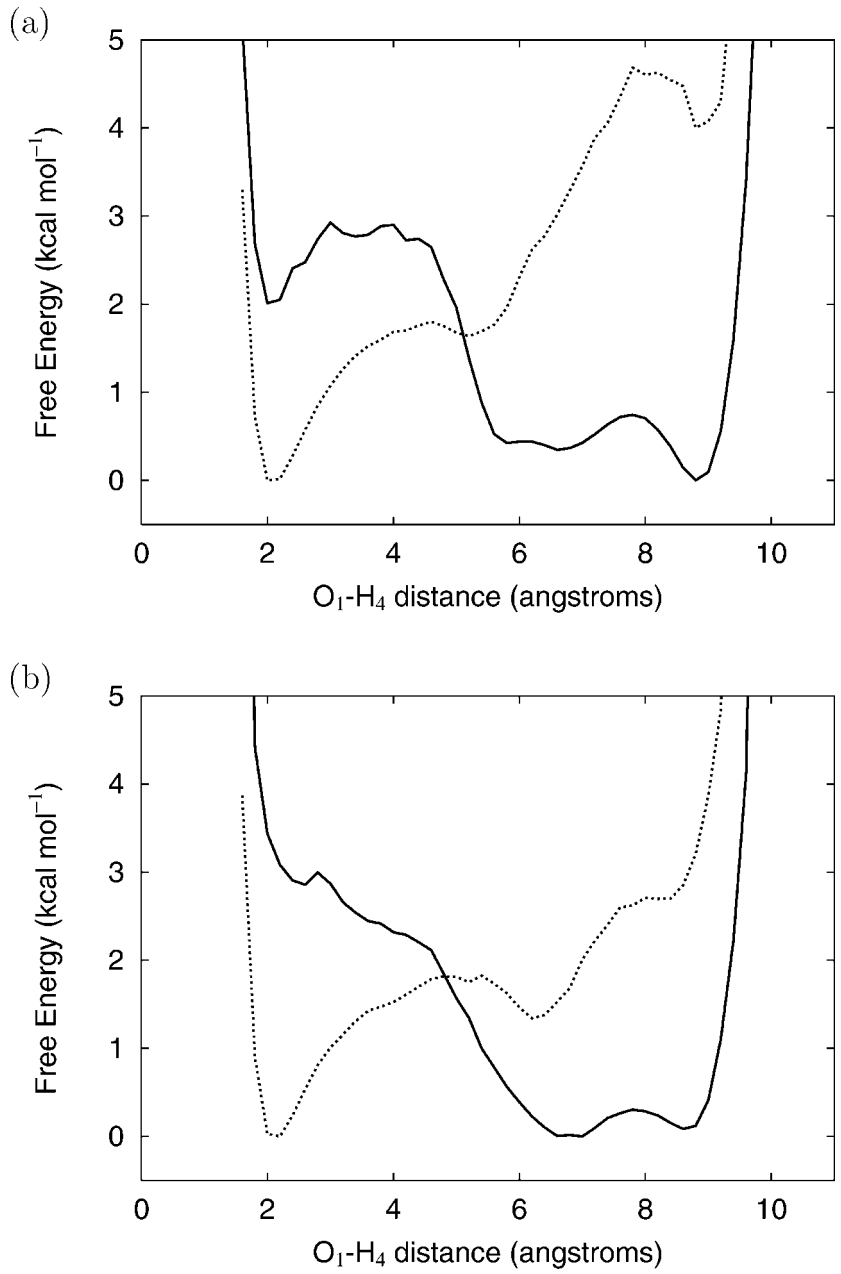

FIGURE 3. Free energy profile along O_i—H_{i+3} ($i = 1$) of Ac-$(Ala)_2$-NMe (a) *in vacuo* and (b) in water for the C96 (solid line) and AMBER95 (dotted line) force fields.

have small peaks around the $C7_{ax}$ region, due to the lack of environmental restrictions for the isolated peptide.

Figure 3b shows the free energy profile of the alanine tripeptide Ac-$(Ala)_2$-NMe in water, in the same manner as Figure 3a. The overall free energy profiles in water were not very different from those *in vacuo*. For the C96 force field, the most remarkable change from *in vacuo* to in water is the almost complete disappearance of the local minimum around O_1—$H_4 =$ 2 Å. In contrast, for the AMBER95 force field, the extended conformation became more stabilized in water than *in vacuo*. With the C96 force field, the most stable conformer is located around 6.6 Å, but the energy difference between 6.6 and 8.8 Å is only 0.1 kcal mol^{-1}, and the energy barrier between the two conformations is only 0.3 kcal mol^{-1}, which is about half of that *in vacuo*.

Figure 6 shows the (ϕ, ψ) probability distribution map in water. Interestingly, the peaks of the α_R re-

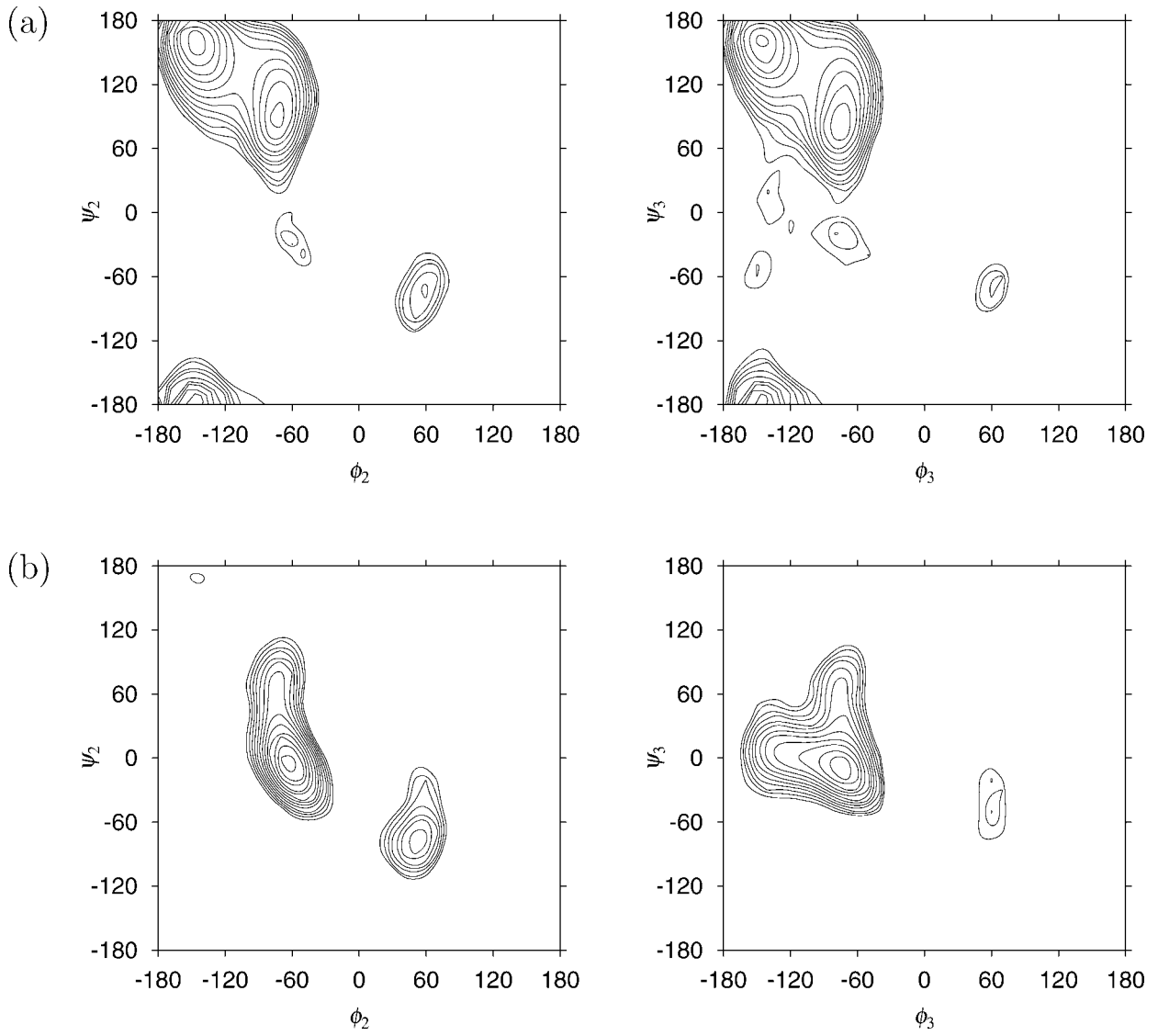

FIGURE 4. Probability distribution of the alanine backbone dihedral angles, ϕ–ψ, in degrees of Ac-$(Ala)_2$-NMe *in vacuo* for (a) C96 and (b) AMBER95. All of the contours are indicated by the common logarithmic scaling, with a contour interval of 0.2.

gion increased substantially for the C96 force field, where the gas phase has only unremarkable small peaks. For AMBER95, the positions of the main peaks around α_R region in water are close to those in the gas phase, and small peaks appeared around the β region in water. No peaks were found around $C7_{ax}$ with either C96 or AMBER95. This may be the result of the interaction between the peptide and the water molecules.

It is interesting to compare our results with those from another force field, which is parameterized from different approaches. The potential of mean force using CHARMM19[7] *in vacuo* has a minimum at 6.2 Å, and is somewhat similar to that of C96 below 6.2 Å. However, above 6.2 Å, the potential of mean force rises sharply and CHARMM19 does not have any stable extended conformations. Tobias et al.[6] studied the same peptide, Ac-$(Ala)_2$-NMe, in TIP3P water for the CHARMM19 force field with periodic boundary conditions and an umbrella sampling method. CHARMM19 in the gas phase destabilized the extended conformer, but in water, the extended conformers were stabilized and the free energy profile was similar to the current result with C96 in water.

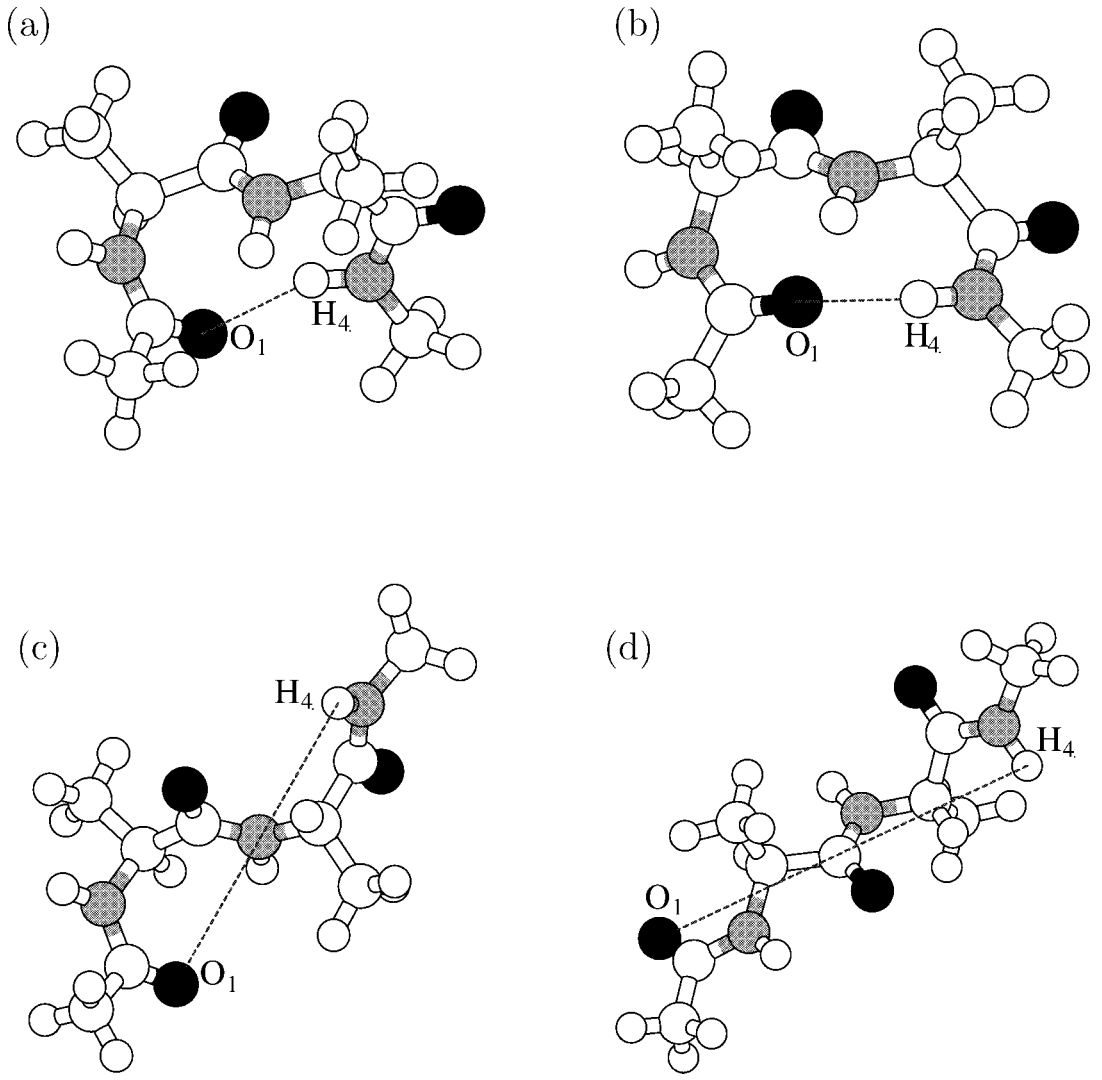

FIGURE 5. Snap shot structures of Ac-$(Ala)_2$-NMe *in vacuo* (a) for AMBER95 with O_1—$H_4 = 2$ Å, (b) for C96 with O_1—$H_4 = 2$ Å, (c) for C96 with O_1—$H_4 = 7$ Å, and (d) for C96 with O_1—$H_4 = 9$ Å. Carbons are white, oxygens are black, nitrogens are gray, and hydrogens are small and white.

ALANINE TETRAPEPTIDE

Figure 7 shows the free energy profiles of the alanine tetrapeptide Ac-$(Ala)_3$-NMe *in vacuo*. For the C96 force field, a local minimum appeared around O_i—$H_{i+3} = 2$ Å for $i = 1$, but not for $i = 2$. Moreover, both profiles also prefer the extended conformers with the local minima at 9 Å. In contrast, for AMBER95, the potential of mean force has a lowest local minimum around O_i—$H_{i+3} = 2$ Å and indicates almost the same free energy profiles for $i = 1$ and $i = 2$, as shown in Figure 7a. Figure 7b shows the free energy profile along the O_1—H_5 distance. For C96, the conformation around 5.6 Å has two hydrogen bonds, mainly between O_1—H_3 and O_3—H_5. For AMBER95, the conformation around 4.4 Å has two successive Type I turns, forming the O_1—H_4 and O_2—H_5 hydrogen bonds. Each force field has a local minimum around 2 Å, where the free energy difference from the most stable conformation is 3.0 kcal mol^{-1} for C96 and 1.9 kcal mol^{-1} for AMBER95, respectively. This indicates that the O_1—H_5 hydrogen bond is more likely to be formed for the AMBER95 force field. From these energy profiles, the C96 force field seems to give a high degree of conformational variety compared to the AMBER95 force field.

In Figure 8, the free energy profiles of Ac-$(Ala)_3$-NMe in water are shown. For the O_i—H_{i+3} distance, almost the same characteristics were observed as

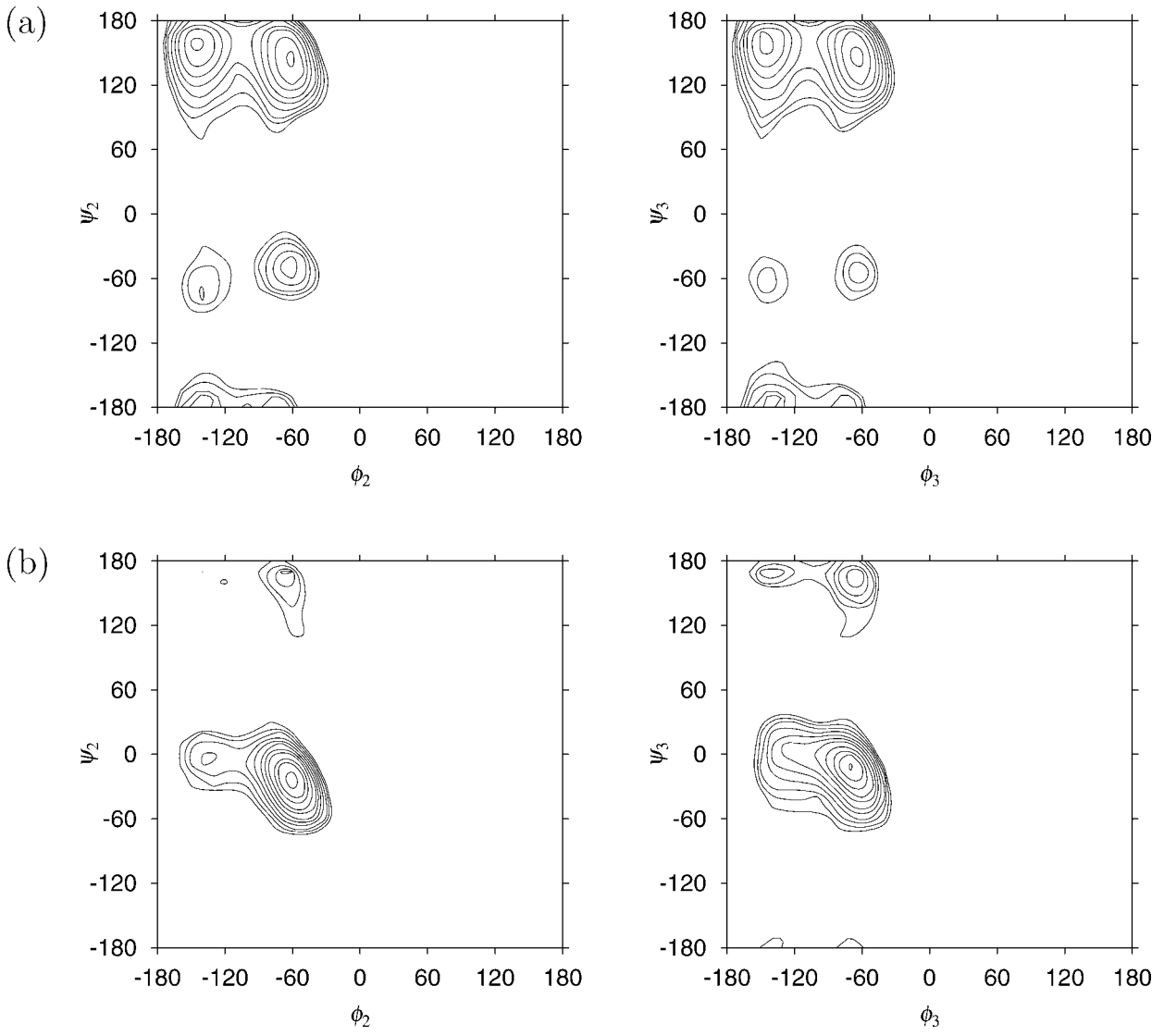

FIGURE 6. Probability distribution of the alanine backbone dihedral angles, ϕ–ψ, in degrees of Ac-$(Ala)_2$-NMe in water for (a) C96 and (b) AMBER95. All of the contours are indicated in the same way as in Figure 4.

those in the case of Ac-$(Ala)_2$-NMe for both the C96 and AMBER95 force fields (see Fig. 8a and Fig. 3b). For the C96, the extended conformation between 7 to 9 Å is most stable, and the compact conformation with the hydrogen bond between O_i and H_{i+3} disappeared compared to the gas phase. In contrast, for AMBER95, the conformation with the hydrogen bond between O_i and H_{i+3} is most preferred, and the stability of the extended states is enhanced compared to the gas phase. This tendency is also shown from the energy surface of the O_1—H_5 distance in Figure 8b. The compact and turn conformers are destabilized for the C96 force field, whereas the hydrogen bonded and extended conformers are stabilized with AMBER95. Figure 9 shows a snap shot of these local minima structures in water. The changes of the (ϕ, ψ) distributions from the isolated gas states to the solvated states (data not shown) are almost the same as those in Ac-$(Ala)_2$-NMe for both C96 and AMBER95, respectively. These results confirm that the extended conformers are favored for C96, and that the Type I turn conformations are favored for AMBER95.

Samuelson et al.[10] calculated the free energy profiles of Ac-$(Ala)_3$-NMe for the AMBER95, CHARMM19, and CHARMM22 force fields with the umbrella sampling method *in vacuo* and in TIP3P water. According to their results, gas phase free energy profiles along the O_1—H_5 distance for AMBER95 agree well. However, in water, their re-

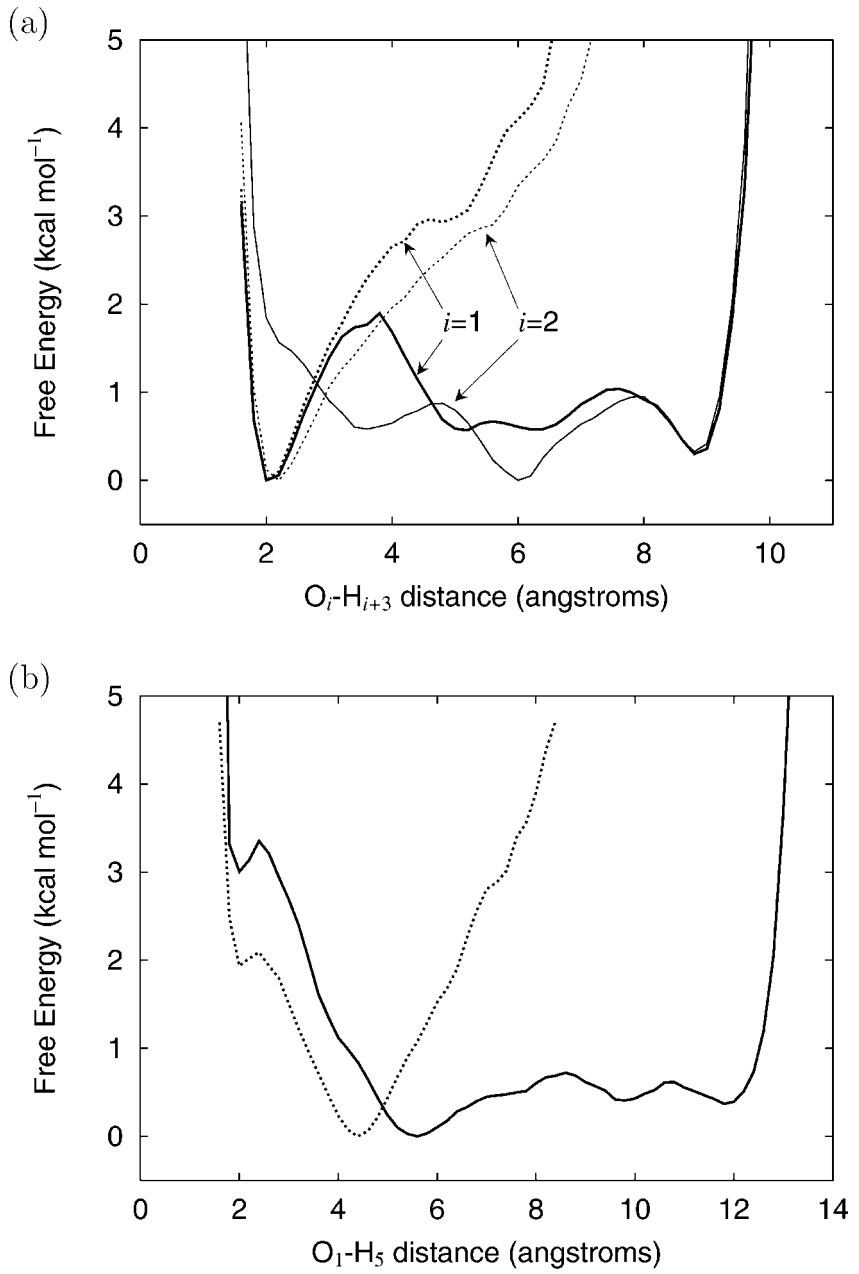

FIGURE 7. Free-energy profile along (a) O_i—H_{i+3} (thick lines for O_1—H_4 and thin lines for O_2—H_5) and (b) O_i—H_{i+4} (O_1—H_5) of Ac-$(Ala)_3$-NMe *in vacuo* for the C96 (solid lines) and AMBER95 (dotted lines) force fields.

sult had no local minimum around O_1—$H_5 = 10$ Å, whereas our result shows a local minimum at 10 Å that is 2.5 kcal mol^{-1} higher than the global minimum. To examine the convergence of our simulation, an additional 10-ns MD run was carried out using AMBER95 with a different initial structure (O_1—$H_5 = 6$ Å). This MD run also yielded flat energy distributions (dashed lines in Fig. 2d), which indicate that the multicanonical ensemble was again produced. In Figure 8b, the free energy profile along the O_1—H_5 distance is plotted with a dashed line, which shows almost the same profile as the original dotted line, and has a local minimum at 10 Å, also. The difference between the Samuelson and the present results could arise from the differences of the sampling methods, the number of water molecules, and the use of cutoff of nonbonded interactions. However, our purpose is not to investigate the difference between such local minima with extremely low probability, but the position of the

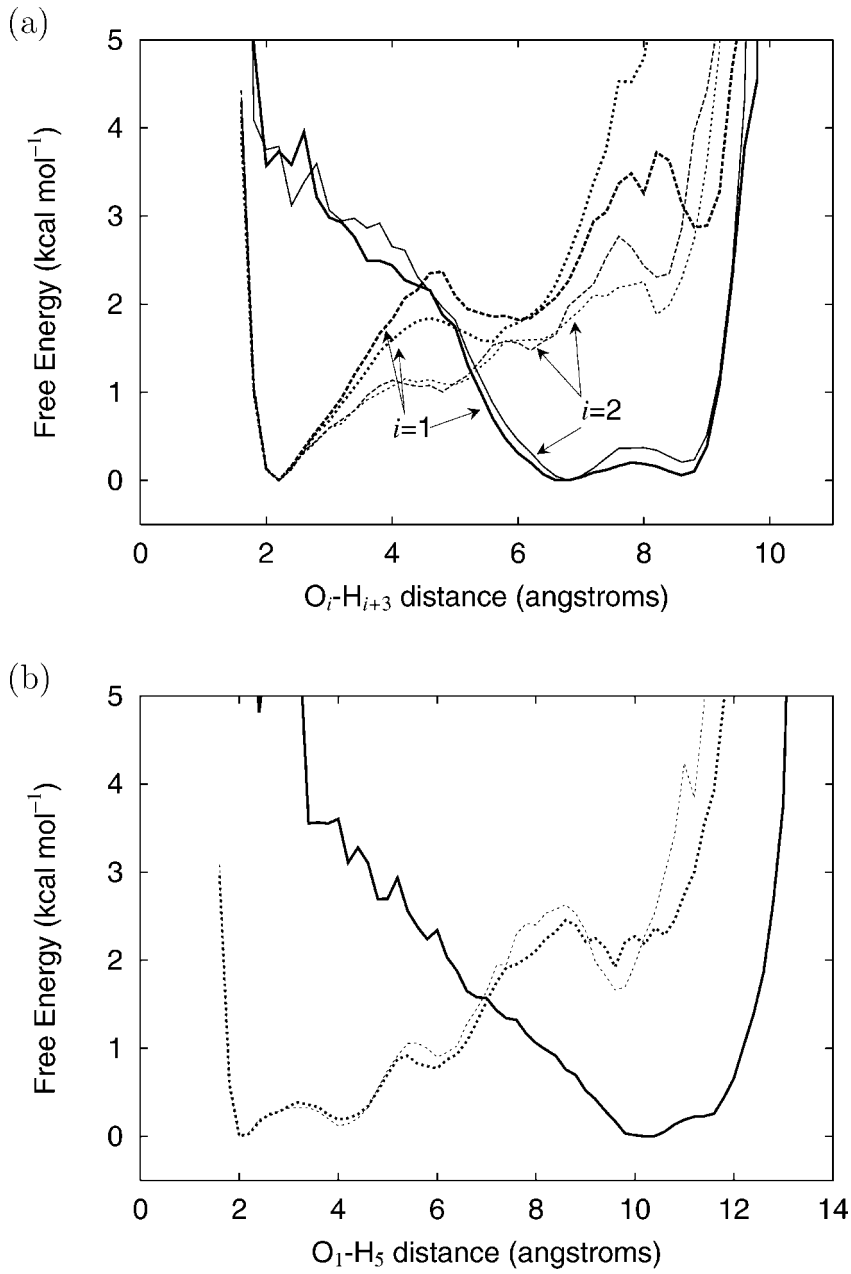

FIGURE 8. Free-energy profile along (a) O_i—H_{i+3} (thick lines for O_1—H_4 and thin lines for O_2—H_5) and (b) O_i—H_{i+4} (O_1—H_5) of Ac-$(Ala)_3$-NMe in water for the C96 (solid lines), AMBER95 (dotted lines) and an additional 10 ns simulation with AMBER95 (dashed lines).

global minima and the local minima with less than 2 kcal mol^{-1}. In this regard, the Samuelson and the present results agree well.

THERMODYNAMIC PROPERTY

To estimate a thermodynamic property of the force fields, the specific heat, C, was calculated from the *in vacuo* trajectories by $C(T) = (\langle E^2 \rangle - \langle E \rangle^2)/RT^2$. Here, E is the energy at temperature, T, $\langle\ \rangle$ indicates ensemble average, and R is the gas constant. Additional simulations for Ac-$(Ala)_4$-NMe *in vacuo* were done, and C was calculated. Figure 10a shows the temperature dependence of the resulting specific heat for $n = 2$, 3 and 4 for both the AMBER95 and C96 force fields. In Figures 10b and c, the energy profile for C96 and AMBER95 are shown. For C96, a peak appears at $T = 250$ K for $n = 3$ and

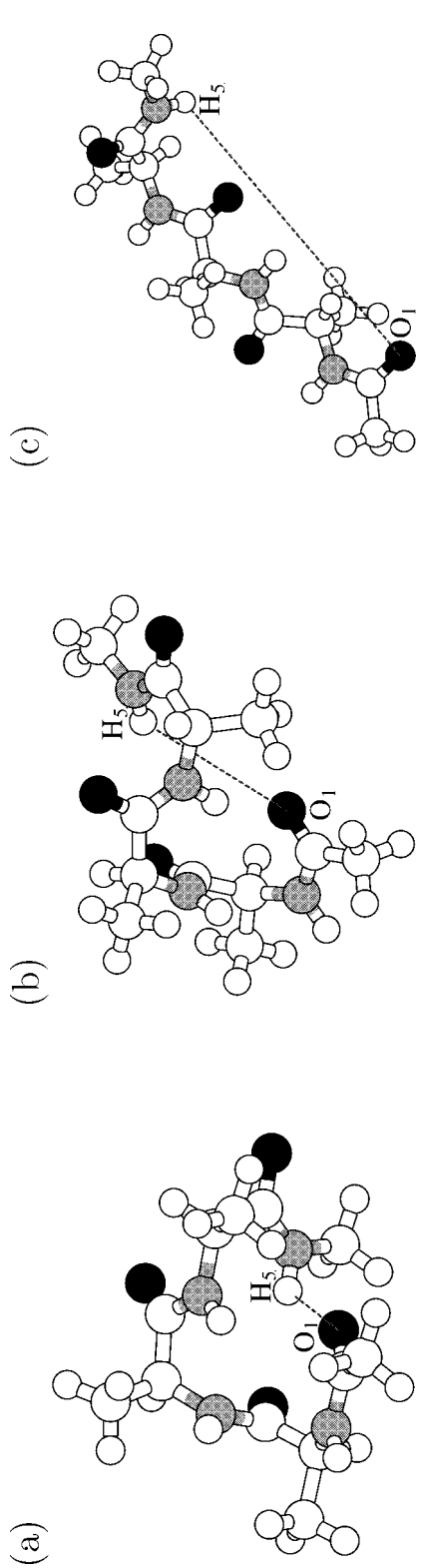

FIGURE 9. Snap shot structures of Ac-(Ala)$_3$-NMe in water (a) for AMBER95 with O_1—H_5 = 2 Å, (b) for AMBER95 with O_1—H_5 = 4 Å, and (c) for C96 with O_1—H_5 = 10 Å.

$T = 400$ K for $n = 4$. No clear peak was observed for AMBER95. These results indicate that the C96 and AMBER95 force fields are thermodynamically different. Remember that the multicanonical simulation is a canonical simulation for the modulated potential surface [eq. (5)] at a given temperature. The energy profile for C96 shows that the conformational space is separated into subspaces, between which free energy barriers exist. The multicanonical conformational sampling is done using a single function for the density of states, which should be regarded as an average over the subspaces. Then, when the conformation is in a subspace, the sampling provides a partly flat energy distribution. After a long simulation, where the conformation can move among the subspaces, these partly flat distributions are integrated into a widely flat distribution.

These results indicate that the C96 force field *in vacuo* has a rugged potential surface, and that AMBER95 has a somewhat funnel-like potential surface. This feature caused a difficulty in the multicanonical sampling with the C96 force field.

Conclusion

The C96 and AMBER95 force fields were compared using the model peptide Ac-(Ala)$_n$-NMe ($n =$ 2 and 3) *in vacuo* and in water by multicanonical molecular dynamics simulations. From the free energy profiles along the reaction coordinates, the distances O_i—H_{i+3} and O_i—H_{i+4}, and the backbone (ϕ, ψ) probability distribution maps, it was concluded that C96 prefers extended conformers, while AMBER95 preferred turn conformers, both *in vacuo* and in water.

Changing only a few dihedral parameters in C96 provides completely different free-energy and specific-heat profiles. This can be understood, however, in terms of the effect on the potential map for the alanyl dipeptide, which shows relative point-to-point differences between AMBER95 and C96 of up to 5 kcal mol^{-1} on balance (Fig. 1c).

This study does not directly address the question of which force field is the more accurate. To fully answer that question, a comparison between the simulations and the experimental results will be required. We note, however, that Samuelson et al.[10] found that the CHARMM22 force field[5] yields a free-energy profile along the O_1—H_5 reaction coordinate that broadly resembles the profile we have found for C96 and that differs substantially from the one we, and they, have found for AMBER95. This suggests that the C96 force field has the similar

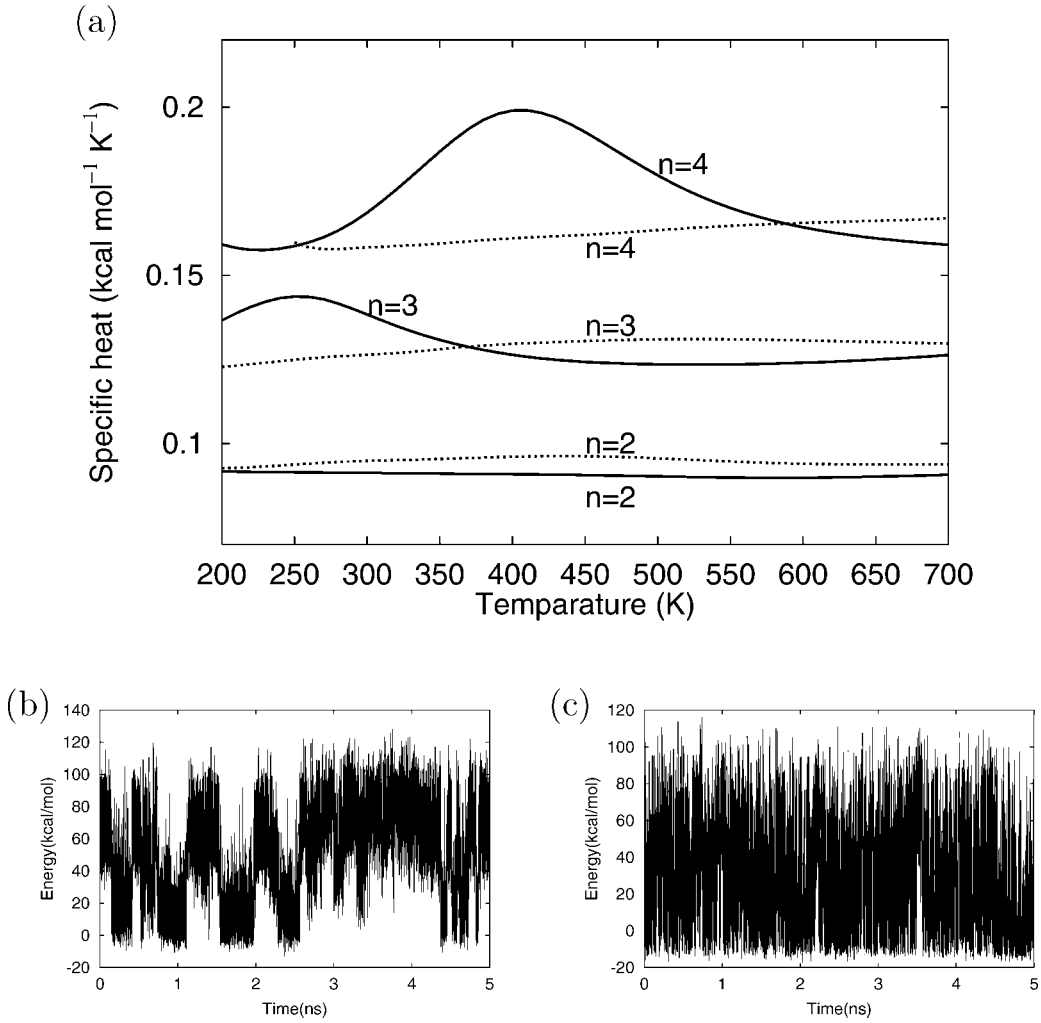

FIGURE 10. (a) Specific heat obtained for Ac-(Ala)$_n$-NMe ($n = 2$ to 4) for C96 (solid line) and AMBER95 (dotted line) *in vacuo*. Energy trajectories of the Ac-(Ala)$_4$-NMe ($n = 4$) *in vacuo* for (b) C96 and (c) AMBER95.

features to the CHARMM22, at least for the structural properties addressed in the present study. Any definitive conclusion must await the availability of pertinent experimental data.

References

1. Cornell, W. D.; Cieplak, P.; Bayly, C. I.; Gould, I. R.; Merz, K. M., Jr.; Ferguson, D. M.; Spellmeyer, D. C.; Fox, T.; Caldwell, J. W.; Kollman, P. A. J Am Chem Soc 1995, 117, 5179.
2. Beachy, M. D.; Chasman, D.; Murphy, R. B.; Halgren, T. A.; Friesner, R. A. J Am Chem Soc 1997, 119, 5908.
3. Kollman, P.; Dixon, R.; Cornell, W.; Fox, T.; Chipot, C.; Pohorille, A. In Computer Simulation of Biomolecular Systems; van Gunsteren, W. F.; Weiner, P. K.; Wilkinson, A. J., Eds.; Kluwer/ESCOM, The Netherlands, 1997, p. 83, Vol. 3.
4. Brooks, C. L., III; Case, D. A. Chem Rev 1993, 93, 2487.
5. MacKerell, A. D., Jr.; Bashford, D.; Bellott, M.; Dunbrack, R. L., Jr.; Evanseck, J. D.; Field, M. J.; Fischer, S.; Gao, J.; Guo, H.; Ha, S.; Joseph–McCarthy, D.; Kuchnir, L.; Kuczera, K.; Lau, F. T. K.; Mattos, C.; Michnick, S.; Ngo, T.; Ngyuen, D. T.; Prodhom, B.; Reiher, W. E., III; Roux, B.; Schlenkrich, M.; Smith, J. C.; Stote, R.; Straub, J.; Watanabe, M.; Wiórkiewicz–Kuczera, J.; Yin, D.; Karplus, M. J Phys Chem B 1998, 102, 3586.
6. Tobias, D. J.; Sneddon, S. F.; Brooks, C. L., III J Mol Biol 1990, 216, 783.
7. Beglov, D.; Roux, B. Biopolymers 1995, 35, 171.
8. Tobias, D. J.; Brooks, C. L., III Biochemistry 1991, 30, 6059.
9. Boczko, E. M.; Brooks, C. L., III J Phys Chem 1993, 97, 4509.
10. Samuelson, S.; Tobias, D. J.; Martyna, G. J. J Phys Chem B 1997, 101, 7592.
11. Berg, B. A.; Neuhaus, T. Phys Lett B 1991, 267, 249.
12. Hansmann, U. H. E.; Okamoto, Y. J Comput Chem 1993, 14, 1333.
13. Hansmann, U. H. E.; Okamoto, Y. Physica A 1994, 212, 415.

14. Okamoto, Y.; Hansmann, U. H. E. J Phys Chem 1995, 99, 11276.
15. Kidera, A. Proc Natl Acad Sci USA 1995, 92, 9886.
16. Hansmann, U. H. E.; Okamoto, Y.; Eisenmenger, F. Chem Phys Lett 1996, 259, 321.
17. Nakajima, N.; Nakamura, H.; Kidera, A. J Phys Chem B 1997, 101, 817.
18. Nakajima, N.; Higo, J.; Kidera, A.; Nakamura, H. Chem Phys Lett 1997, 278, 297.
19. Shirai, H.; Nakajima, N.; Higo, J.; Kidera, A.; Nakamura, H. J Mol Biol 1998, 278, 481.
20. Nakajima, N. Chem Phys Lett 1998, 288, 319.
21. Morikami, K.; Nakai, T.; Kidera, A.; Saito, M.; Nakamura, H. Comput Chem 1992, 16, 243.
22. Jorgensen, W. L.; Chandrasekhar, J.; Madura, J. D.; Impey, R. W.; Klein, M. L. J Chem Phys 1983, 79, 926.
23. Evans, D. J.; Morriss, G. P. Phys Lett A 1983, 98, 433.
24. Hoover, W. G.; Ladd, A. J. C.; Moran, B. Phys Rev Lett 1982, 48, 1818.
25. Ryckaert, J. P.; Ciccotti, G.; Berendsen, H. J. C. J Comput Phys 1977, 23, 327.